New Physics: Sae Mulli,
Vol. 68, No. 12, December 2018, pp. 1324∼1330
http://dx.doi.org/10.3938/NPSM.68.1324

Analysis of α + ^{40}Ca and α + ^{58}Ni Elastic Scatterings at E_{lab} = 240 MeV

Yong Joo KIM*
Department of Physics and Research Institute for Basic Sciences, Jeju National University, Jeju 63243, Korea

(Received 11 September 2018 : accepted 10 October 2018)

The elastic scatterings for the α + ^{40}Ca and the α + ^{58}Ni systems at E_{lab} = 240 MeV have been analyzed within the framework of the Coulomb-modified Glauber model using two kinds of Gaussian density parameters for the target nuclei. The first one is to use Gaussian density parameters obtained from the root-mean-square radius. The second one is to use parameters calculated by matching the Gaussian density to the two-parameter Fermi density. The results with surface-matched Gaussian densities provide reasonable agreement with the experimental data, but the results without matching do not. The oscillatory structures observed in the angular distributions of both system can be interpreted as being due to the strong interference between the near-side and the far-side scattering amplitudes. The differences between the phase shifts obtained from the two methods are examined. We also investigate the effect of these differences on the differential and reaction cross sections, the transmission functions and the strong absorption radii.

PACS numbers: 25.70.-z, 25.55.Ci
Keywords: Coulomb-modified Glauber model, Surface-matched Gaussian density, Elastic scattering, α+^{40}Ca, α+^{58}Ni

I. INTRODUCTION

Optical limit approximation (OLA) to the Glauber model has been used in the description of elastic scattering data at high energies. In the simple Glauber approach to heavy-ion elastic scattering [1], it is assumed that the flux attenuation of the elastic channel occurs by means of nucleon-nucleon collisions along a classical straight line trajectory. This is not a good approximation at relatively low and intermediate energies. The conventional form of the Glauber model was modified [2,3] to account for the deviation of the projectile trajectory due to the Coulomb field. This type of OLA to the Glauber model is called as "Coulomb-modified Glauber model (CMGM)". A modified Glauber model taking into account the deflection effect of the trajectory due to the real nuclear potential was reported [4,5]. Charagi and Gupta [6] have extended the CMGM to lower energies for the description of the differential cross section.

The ingredients in the nuclear phase shift of the CMGM are the densities of colliding nuclei and the elementary nucleon-nucleon (NN) scattering amplitude. The nuclear densities are usually assumed as Gaussian shape, which have an advantage of yielding an analytic expression for the nuclear phase shift. In the case of heavier nuclei ($A \geqq 40$), realistic density distributions are required to describe the tapered nuclear surface. Karol [7] has obtained the Gaussian density parameters by fitting the realistic density to reproduce the experimentally determined nuclear surface texture. Meanwhile, Charagi and Gupta [8] have obtained the Gaussian density parameters by matching the Gaussian density profile function to the 2-parameter Fermi profile function. The elastic scattering angular distributions of ^{16}O + ^{16}O system at E_{lab} = 350 and 480 MeV has been analyzed within the framework of CMGM by matching the Gaussian density parameters to the modified Fermi ones [9].

In this paper, we analyze the elastic scatterings of α + ^{40}Ca and α + ^{58}Ni systems at E_{lab} = 240 MeV by using the Gaussian density parameters for the target nuclei

*E-mail: yjkim@jejunu.ac.kr

matched to the 2-parameter Fermi (2pF) density following the Karol method [7]. The calculated results will be compared to the ones without surface-matched Gaussian densities. Further, we investigate the differences between the phase shifts obtained from the Gaussian density with and without matching to the 2pF density, and how these differences produce an effect on the (differential and reaction) cross sections, transmission functions and strong absorption radii. The Coulomb-modified Glauber model is briefly described in Sec. II. In Sec. III, we present the theory related with the calculation processes of the Gaussian density parameters by matching the Gaussian density to the 2pF density. Section IV is devoted to the results and discussion, in which we perform a CMGM analysis for α + ^{40}Ca and α + ^{58}Ni elastic scatterings at E_{lab} = 240 MeV. Finally, we provide the concluding remarks in Sec. V.

II. COULOMB-MODIFIED GLAUBER MODEL

In the optical limit approximation to the Glauber model, the nuclear phase shift $\delta(b)$ for the scattering of a projectile nucleus of mass number A_P on a target nucleus of mass number A_T may be written as [10,11]

$$\delta(b) = \frac{A_P A_T}{2k_{NN}} \int_0^\infty dqq J_0(qb) f_{NN}(q) F_P(q) F_T(q), \quad (1)$$

where q is the momentum transfer, k_{NN} is the nucleon momentum corresponding to the projectile kinetic energy per nucleon, $J_0(qb)$ is the Bessel function of zeroth order, $F_P(q)$ and $F_T(q)$ are the projectile (P) and target (T) form factors, and $f_{NN}(q)$ is NN scattering amplitude. If we assume nuclear density $\rho_i(r)$ as a Gaussian form

$$\rho_i(r) = \rho_i(0) \exp(-\frac{r^2}{a_i^2}), \quad i = P, T \quad (2)$$

and use the Fourier transformation of $\rho_i(r)$, the nuclear form factor is expressed as

$$F_i(q) = (\sqrt{\pi} a_i)^3 \rho_i(0) \exp(-q^2 a_i^2/4). \quad (3)$$

For the $f_{NN}(q)$, we take Gaussian parametrization of the form [12] :

$$f_{NN}(q) = \frac{k_{NN}}{4\pi} \sigma_{NN}(\alpha_{NN} + i) \exp[-\beta_{NN} q^2/2], \quad (4)$$

where σ_{NN} is the NN total cross section, α_{NN} is the ratio of the real to imaginary parts of the forward NN scattering amplitude, and β_{NN} is the slope parameter. Inserting Eqs. (3) and (4) into Eq. (1), an analytic expression of the nuclear phase shift can be obtained as

$$\delta(b) = \frac{A_P A_T}{4R^2} \pi^2 a_P^3 a_T^3 \rho_P(0) \rho_T(0) \sigma_{NN}(\alpha_{NN}+i) \exp[-\frac{b^2}{R^2}], \quad (5)$$

where

$$R^2 = a_P^2 + a_T^2 + 2\beta_{NN}. \quad (6)$$

One of the basic assumptions of the conventional Glauber model is that the projectile follows a straight line trajectory during a collision with the target nucleus. For the Coulomb-modified Glauber model taking into the Coulomb field, the impact parameter $b = \sqrt{L(L+1)}/k$ is replaced by the distance of closest approach r_c [12]:

$$r_c = \frac{1}{k}(\eta + \sqrt{\eta^2 + L(L+1)}), \quad (7)$$

where η is the Sommerfeld parameter. Then the nuclear phase shift $\delta(b)$ in Eq. (5) can be replaced by an expression $\delta_L(r_c)$ in terms of angular momentum L.

The elastic scattering amplitude for spin-zero charged particle on target nucleus may be written as

$$f(\theta) = f_R(\theta) + \frac{1}{ik} \sum_{L=0}^{\infty} (L+\frac{1}{2}) \exp(2i\sigma_L)(S_L - 1) P_L(\cos\theta), \quad (8)$$

where $f_R(\theta)$ is the usual Rutherford scattering amplitude, σ_L is the Coulomb phase shift, k is the wave number of the system, $P_L(\cos\theta)$ is the Legendre polynomial, and S_L is the nuclear scattering matrix element given by

$$S_L = \exp[2i\delta_L(r_c)]. \quad (9)$$

III. GAUSSIAN DENSITY PARAMETERS

For the light nuclei, with $A < 40$, the density distribution is usually assumed to be Gaussian form of Eq. (2). The Gaussian density parameters $\rho_i(0)$ and a_i are related with the root-mean-square radius R^i_{rms} by

$$a_i = \frac{R^i_{rms}}{\sqrt{1.5}}, \quad \rho_i(0) = \frac{1}{(a_i\sqrt{\pi})^3}, \quad (10)$$

Table 1. Input parameters and χ^2/N values in the Coulomb-modified Glauber model using Gaussian density parameters $\rho_T(0)$ and a_T obtained by matching the Gaussian density to the 2-parameter Fermi density [13] for the $\alpha + {}^{40}$Ca and $\alpha + {}^{58}$Ni elastic scatterings at $E_{lab} = 240$ MeV. We used $\rho_P(0) = 0.06598\ fm^{-3}$ and $a_P = 1.396\ fm$ obtained from the root-mean square radius [14]. An asterisk (*) indicates the best fitted parameters (α_{NN}) and corresponding χ^2/N values by using CMGM without surface-matched Gaussian density. The χ^2/N values in parentheses are the results using $\rho_T(0)$ and a_T calculated from the R_{rms} radii [13].

Target	σ_{NN} (mb)	R_{rms} (fm)	$\rho_T(0)$ (fm^{-3})	a_T (fm)	β_{NN} (fm^2)	α_{NN}			χ^2/N^a
^{40}Ca	68.3	3.399	0.01856	2.443	0.5318	1.646*	1.557	8.75*	5.54 (9.45)
^{58}Ni	68.3	3.753	0.01673	2.631	0.5318	1.322*	1.336	4.14*	3.38 (4.19)

[a] 10% error bars, $\chi^2/N = (1/N)\sum_{i=1}^{N}\left[\frac{\sigma_{\rm th}(\theta_i)-\sigma_{\rm ex}(\theta_i)}{\Delta\sigma_{\rm ex}(\theta_i)}\right]^2$

where the Gaussian density distribution is normalized to unity. But for heavier nuclei ($A \geqq 40$), realistic density distribution is needed for describing the tapered nuclear surface. To obtain an analytic expression for the nuclear phase shift of Eq. (5), it is necessary to match the Gaussian density distribution to the realistic density one in nuclear surface.

The 2-parameter Fermi (2pF) form for the nuclear densities is given as

$$\rho_i^{2pF}(r) = \frac{\rho_i^{2pF}(0)}{1+\exp[(r-c_i)/d_i]}, \tag{11}$$

where

$$\rho_i^{2pF}(0) = \left[4\pi\int_0^\infty \frac{1}{1+\exp[(r-c_i)/d_i]} r^2 dr\right]^{-1}. \tag{12}$$

As suggested by Karol [7], the parameters $\rho_i(0)$ and a_i in Eq. (2) are calculated by requiring $\rho_i(r)$ at $r = c_i$ and $r = c_i + t_i/2$ in the Gaussian distribution to be identical to the values calculated from the 2pF distribution where c_i is the half-central-density radius and $t_i = 4.4d_i$ is the 90% - 10% surface skin thickness parameter. Consequently, the parameters for the surface matched Gaussian densities are obtained as follows [7]:

$$\rho_i(0) = \frac{1}{2}\rho_i^{2pF}(0)\exp(\frac{c_i^2}{a_i^2}). \tag{13}$$

and

$$a_i = \left[\frac{4c_it_i + t_i^2}{4(\ln 5)}\right]^{1/2}. \tag{14}$$

For the target nuclei, two methods are employed to calculate the Gaussian density parameter values of $\rho_T(0)$ and a_T. The first one (Cal. 1) is simply to use the Eq. (10) obtained from R_{rms}^i. The second one (Cal. 2) is to use the Eqs. (13) and (14) which match Gaussian densities to the 2pF ones. Parameter values of the surface-matched Gaussian density for the target nuclei are listed in Table 1 along with the R_{rms}^i. In Fig. 1, we gave a plot of the Gaussian and 2pF density distributions for ^{40}Ca and ^{58}Ni target nuclei. In this figure, the nuclear

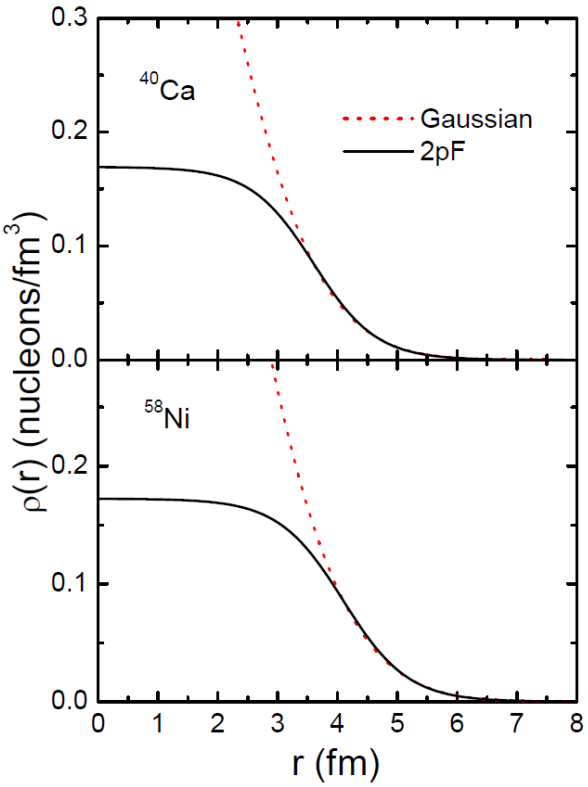

Fig. 1. (Color online) Gaussian and 2-parameter Fermi density distributions for ^{40}Ca and ^{58}Ni target nuclei. The solid curves denote the results for the 2-parameter Fermi density [13] and the dotted curves are the results for the Gaussian one. The nuclear density distributions are normalized to the total number of nucleons.

density distributions are normalized to the total number of nucleons. The solid curves denote the results for 2pF density distributions Eq. (11) using the parameters c_i and d_i taken from Ref. [13], whereas the dotted curves are the results for Gaussian density ones Eq. (2) using the surfaced-matched parameters Eqs. (13) and (14). We can see in this figure that the agreements between the 2pF and the fitted Gaussian density distributions are satisfactory in surface region, though two curves were shown to be greatly different in the central regions. Since most of the contributions to the differential cross section comes from the surface region of the colliding nuclei, the big discrepancies at the central regions between two curves can be neglected.

IV. RESULTS AND DISCUSSION

The elastic differential cross sections for 240 MeV α particles on ^{40}Ca and ^{58}Ni targets have been calculated using the Coulomb-modified Glauber model described in the previous sections. The inputs required for calculation are the parameters $\rho_i(0)$ and a_i of Gaussian density, and σ_{NN}, α_{NN} and β_{NN} of NN amplitude. The parameters $\rho_P(0)$ and a_P for the projectile are obtained from Eq. (10), where R^i_{rms} are taken from Ref. [14]. The NN total cross section σ_{NN} was obtained from Eq. (3) of Ref. [1] and Eq. (2) of Ref. [15] with $\rho = 0.15\ fm^{-3}$ instead of using experimental values. Regarding the slope parameter β_{NN}, we use $\beta_{NN} = 0.5318\ fm^2$, which was interpolated from the β_{NN} values at 45 and 100 MeV/nucleon [14].

The calculations of elastic differential cross sections have been performed using the CMGM with and without matching to the 2pF density distribution of target nuclei. The results of the differential cross sections for the α + ^{40}Ca and α + ^{58}Ni elastic scatterings at E_{lab} = 240 MeV are depicted in Fig. 2 together with those measured experimentally. The experimental data are taken from Ref. [16,17]. In this figure, the dotted and solid curves are the results using the Gaussian densities without and with matching to 2pF density distributions, respectively. As a whole, dotted curves are slightly shifted to the left and show somewhat lower values at large angles, in comparison with the solid curves. However, by matching the

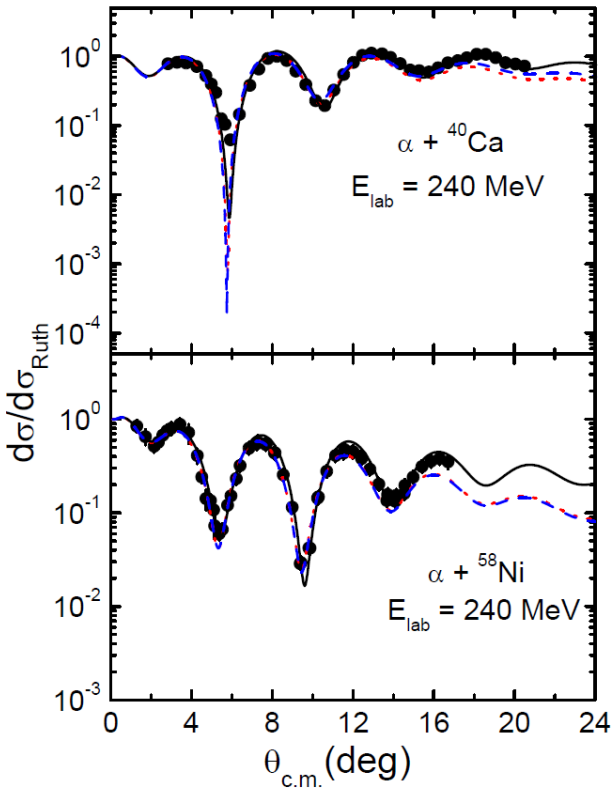

Fig. 2. (Color online) Elastic scattering angular distributions for the α + ^{40}Ca and α + ^{58}Ni systems at E_{lab} = 240 MeV. The solid circles denote the observed data taken from Ref. [16,17]. The solid and dotted curves are the calculated results obtained from the CMGM with and without the surface-matched Gaussian densities. The dashed curves are the best results using the CMGM without the surface-matched Gaussian densities.

Gaussian density to the 2pF one, the dotted curves are moved upward direction at large angles, consequently, leading to fairly good agreements with the experimental data. It can further be seen in Table 1 and Fig. 2 that the results calculated from the surface-matched Gaussian density parameters provided better fits with the experimental data (especially at large angles) than the results from non-surfaced-matched ones.

To examine the necessity of matching the 2pF density in nuclear surface to a Gaussian density, we have also performed a CMGM calculation with Eq. (10) by adjusting the parameters α_{NN} to get best possible fit to the data. The best results are shown in Fig. 2 by the dashed curves and the corresponding α_{NN} parameters are listed in Table 1. As Fig. 2 and Table 1 show, the dashed curves show similar structures to the dotted curves, though dashed curves provide somewhat lower

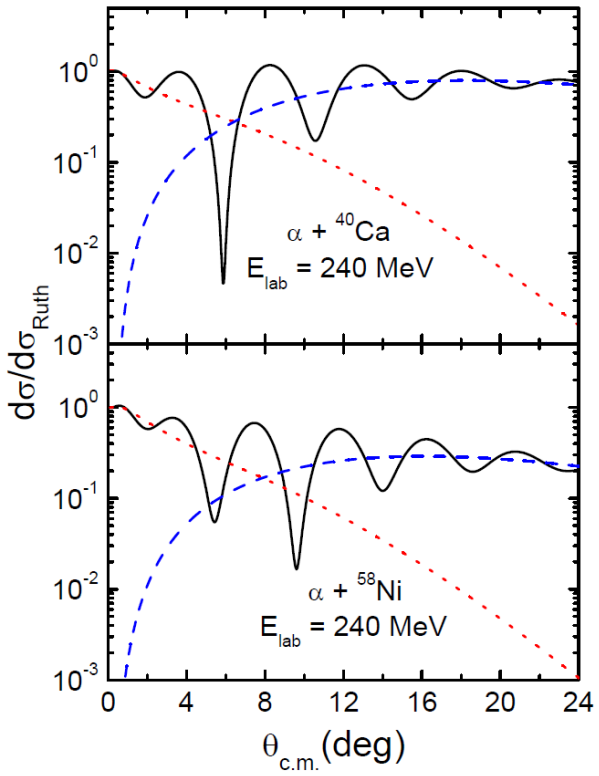

Fig. 3. (Color online) Differential cross sections (solid curves), near-side contributions (dotted curves), and far-side contributions (dashed curves) following Fuller's formalism [18] obtained from the Coulomb-modified Glauber model with the surface-matched Gaussian densities for α + ^{40}Ca and α + ^{58}Ni elastic scatterings at E_{lab} = 240 MeV.

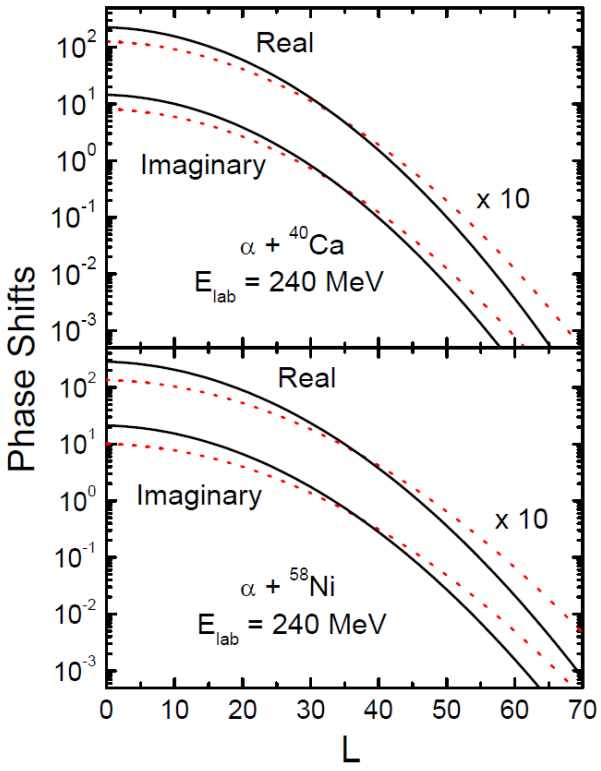

Fig. 4. (Color online) Real and imaginary parts of the phase shifts obtained from the CMGM with (solid curves) and without (dotted curves) the surface-matched Gaussian densities for α + ^{40}Ca and α + ^{58}Ni elastic scatterings at E_{lab} = 240 MeV.

χ^2/N than dotted ones. It is seen that the agreements between solid curves and experimental data are improved for α + ^{40}Ca and α + ^{58}Ni systems at E_{lab} = 240 MeV, in comparison with the results with dashed ones. We find in Table 1 that χ^2/N values obtained from surface-matched Gaussian density parameters are smaller than those from non-surface-matched ones. The improved agreements with the elastic data indicate that the use of the surface-matched Gaussian density is important in the description of elastic scattering involving heavy nucleus.

In order to understand the nature of angular distributions for α + ^{40}Ca and α + ^{58}Ni systems at E_{lab} = 240 MeV, the near-side and the far-side decompositions of the scattering amplitude with the surface-matched Gaussian densities were also performed by following the Fuller's formalism [18]. The contributions of the near-side (dotted curves) and far-side (dashed curves) components to the elastic scattering cross sections are shown in Fig. 3 along with the differential cross sections (solid curves). This figure shows that the near-side contributions dominate for small angles, and the far-side ones for large angles. The near-side and the far-side contributions to the elastic cross sections have equal magnitude at the crossing angles θ_{cross} = 6.40° for α + ^{40}Ca and θ_{cross} = 7.85° for α + ^{58}Ni. The differential cross section is not just a sum of the near-side and the far-side cross sections but contains the interference between the near-side and far-side amplitudes as shown in Fig. 3. The oscillatory structures observed in the angular distributions of both system are due to the strong interference between the near- and the far-side components. The interference oscillations have maximum amplitudes near those crossing angles due to enhanced far-side ones. The behaviors of large-angle cross sections are mainly determined by the far-side amplitude.

As well known, the nuclear phase shift is very important ingredient in describing the elastic cross sections. We plotted in Fig. 4 the real and imaginary parts of

Table 2. Phase shift analysis results from the Gaussian density parameters with (Cal. 2) and without (Cal. 1) matching the Gaussian density to the 2-parameter Fermi density for the α+^{40}Ca and α+^{58}Ni elastic scatterings at E_{lab} = 240 MeV.

Target	Cal. 1		Cal. 2	
	^{40}Ca	^{58}Ni	^{40}Ca	^{58}Ni
θ_{cross} (deg)			6.40°	7.85°
$L_{1/2}$	38.24	43.41	37.56	42.23
R_s (fm)	6.421	7.107	6.311	6.921
σ_{R_s} (mb)	1295	1587	1251	1505
σ_R (mb)	1312	1588	1258	1492

the nuclear phase shift for α + ^{40}Ca and α + ^{58}Ni systems at E_{lab} = 240 MeV. In this figure, the dotted and solid curves are the phase shifts by using the Gaussian parameters without and with matching the 2pF densities. As a whole, the phase shifts obtained from surface-matched Gaussian density parameters produce higher values at small L and lower ones at large L, in comparison with the ones from non-surface-matched ones. As Fig. 4 shows, the solid curves decrease more rapidly compared to the dotted ones so that two curves have equal magnitude at $L \sim 34$ for α + ^{40}Ca and $L \sim 37$ for α + ^{58}Ni. One notices that solid curves have somewhat lower values around the critical angular momentum $L_{1/2}$ corresponding to surface collision, for which $|\exp(-Im[2\delta_L(r_c)])|^2 = 1/2$, in comparison with the dotted curves. Since the elastic scattering cross sections are sensitive mainly to the surface region, the differences of phase shift around $L_{1/2}$ produce somewhat different behaviors of elastic angular distributions.

Such difference of phase shifts has an influence on the transmission function $T_L = 1 - |S_L|^2$. The T_L functions are plotted in Fig. 5 as a function of angular momentum L. The transmission function provides a picture of the absorption in the surface region. As expected, the transmission functions obtained from phase shifts with surface-matched Gaussian density parameters (solid curves) show more rapidly decreasing shape compared to the ones from those without surface-matched ones (dotted curves) around surface regions, consequently producing slightly smaller critical angular momentum ($L_{1/2}$). A further investigation of the situation can be gained by looking at the strong absorption radius (R_s) and the reaction cross sections (σ_{R_s} and σ_R). The R_s is defined

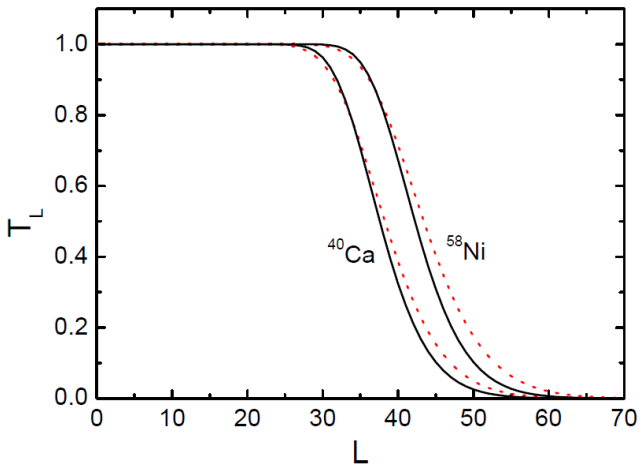

Fig. 5. (Color online) Transmission functions T_L obtained from the CMGM with (solid curves) and without (dotted curves) the surface-matched Gaussian densities for α + ^{40}Ca and α + ^{58}Ni elastic scatterings at E_{lab} = 240 MeV.

as the distance of closest approach determined from the formula $R_s = \{\eta + \sqrt{\eta^2 + L_{1/2}(L_{1/2}+1)}\}/k$, and also reflected in the reaction cross section. The values of $L_{1/2}$,R_s are listed in Table 2 along with the ones of σ_{R_s} and σ_R. As this Table shows, the geometrical reaction cross sections ($\sigma_{R_s} = \pi R_s^2$) are comparable to the ones σ_R obtained from partial wave sum, which is determined by $\sigma_R = (\pi/k^2)\sum_{L=0}^{\infty}(2L+1)T_L$. We can see that the R_s and the σ_R obtained from the surface-matched Gaussian densities are somewhat less than the ones from the non-surface-matched ones.

V. CONCLUDING REMARKS

An analysis of α + ^{40}Ca and α + ^{58}Ni elastic scattering data at E_{lab} = 240 MeV have been made within the framework of the Coulomb-modified Glauber model using two kinds of Gaussian density parameters for the target nuclei: one is obtained from root-mean-square radius, and the other is from matching the Gaussian density to the 2-parameter Fermi density. The calculations using two kinds of Gaussian density parameters for elastic differential cross sections have been compared. We have found that the calculated results obtained from the surface-matched Gaussian density parameters reproduced reasonably well the elastic cross section structure,

and gave better fits with the experimental data, in comparison with the results from non-surface-matched ones. This tell us the necessity of the use of surface-matched Gaussian density in the analysis of elastic scattering involving heavy nucleus. Through the near-side and the far-side decompositions of the elastic cross section, the oscillatory structures observed in the angular distributions of both system are considered to be due to strong interference between the near-side and the far-side scattering components. The behaviors of the large-angle cross sections are attributed to the dominance of the far-side scattering.

The phase shifts from the surface-matched Gaussian density decrease more rapidly and have somewhat lower values around the critical angular momentum $L_{1/2}$, compared to the results from non-surface-matched ones. We can infer that the differences of phase shift around $L_{1/2}$ produced somewhat different behaviors of elastic cross sections because most of the contributions to the differential cross sections are comes from the surface region. Such behaviors of phase shift reflected also in the strong absorption radii and the reaction cross sections. The strong absorption radii and the reaction cross sections using the surface-matched Gaussian density parameters gave somewhat lower values than the results using non-surface-matched ones. These changes are thought to be occurred by the behavior of imaginary phase shift in the surface region around the critical angular momentum $L_{1/2}$.

ACKNOWLEDGEMENTS

This research was supported by the 2018 scientific promotion program funded by Jeju National University.

REFERENCES

[1] J. Chauvin, D. Lebrun, A. Lounis and M. Buenerd, Phys. Rev. C **28**, 1970 (1983).
[2] A. Vitturi and F. Zardi, Phys. Rev. C **36**, 1404 (1987).
[3] S. M. Lenzi, A. Vitturi and F. Zardi, Phys. Rev. C **38**, 2086 (1988).
[4] M. H. Cha and Y. J. Kim, J. Phys. G : Nucl. Part. Phys. **18**, L183 (1992).
[5] Y. J. Kim and M. H. Cha, J. Korean Phys. Soc. **27**, 444 (1994).
[6] S. K. Charagi, Phys. Rev. C **48**, 452 (1993).
[7] P. J. Karol, Phys. Rev. C **11**, 1203 (1975).
[8] S. K. Charagi and S. K. Gupta, Phys. Rev. C **41**, 1610 (1990).
[9] M. H. Cha and Y. J. Kim, Sae Mulli **40**, 183 (2000).
[10] I. Ahmad, M. A. Abdulmomen and M. A. Alvi, Int. J. Mod. Phys. E **11**, 519 (2002).
[11] I. Ahmad and M. A. Alvi, Int. J. Mod. Phys. E **13**, 1225 (2004).
[12] S. Ahmad, A. A. Usmani, S. Ahmad and Z. A. Khan, Phys. Rev. C **95**,054601 (2017).
[13] M. E. Farid and M. A. Hassanain, Nucl. Phys. A **678**, 39 (2000).
[14] M. M. H. El-Gogary, A. S. Shalaby, M. Y. Hassan and A. M. Hegazy, Phys. Rev. C **61**, 044604 (2000).
[15] C. Xiangzhou, F. Jun, S. Wenqing, M. Yugang and W. Jiansong *et al.*, Phys. Rev. C **58**, 572 (1998).
[16] H. L. Clark, Y. W. Lui and D. H. Youngblood, Nucl. Phys. A **589**, 416 (1995).
[17] D. H. Youngblood, Y. W. Lui and H. L. Clark, Phys. Rev. C **55**, 2811 (1997).
[18] R. C. Fuller, Phys. Rev. C **12**, 1561 (1975).